AIAA 81-1290R

Development of a Linear Unsteady Aerodynamic Analysis for Finite-Deflection Subsonic Cascades

Joseph M. Verdon* and Joseph R. Caspar*
United Technologies Research Center, East Hartford, Conn.

A linear unsteady potential flow analysis, which accounts for the effects of blade geometry and steady turning, is being developed to predict the aerodynamic response to blade vibrations in the fan, compressor, or turbine stages of modern jet engines. In previous work numerical solutions were restricted to cascades of sharp-edged blades aligned with the mean flow. Under the present phase of this research the solution procedure has been extended to treat blades with rounded or blunt edges. As part of this effort an analytical model-problem study has been conducted to clarify the behavior of first-order perturbation solutions in the vicinity of airfoil edges. Further, a numerical approximation using concepts from singular perturbation theory has been developed to resolve the unsteady boundary value problem for cascades of blunt leading-edged blades. Numerical results for NACA 0012 cascades, including detailed results in the vicinity of a blade leading edge, are presented and evaluated.

Introduction

A RESEARCH program is being conducted to develop an aerodynamic analysis for predicting unsteady flow in a compressor or turbine blade passage.[1,2] This analysis is intended to serve eventually as the aerodynamic component of a flutter or resonant stress design prediction system for turbomachinery blade rows. To date, the effort has been concentrated on the subsonic flutter or free-vibration problem, but extensions of the analysis to treat transonic flows and forced aerodynamic excitations are planned as future work. Although interest here is focused on cascades, the basic aerodynamic formulation described in this paper should also provide an efficient method for calculating the unsteady forces associated with the motions of a variety of aerodynamic configurations including those of thick, blunt-nosed transonic airfoils.

To overcome the limitations of classical linear theory (e.g., flat plate blades, uniform mean flow, etc.) an aerodynamic model has been formulated which includes the effects of blade geometry and flow turning on unsteady response.[1] Here the unsteady flow is considered as a small-amplitude harmonic fluctuation about nonuniform steady flow. An asymptotic expansion of the time-dependent velocity potential then provides equations which govern the steady and small-disturbance unsteady flows in a single, extended, blade-passage region of the cascade. The steady flow is determined as a solution of the full-potential equation and the unsteady flow is governed by linear equations with variable coefficients which depend on the steady flow. Similar linearizations with respect to a nonuniform mean flow have and are being developed for turbomachinery applications by Atassi and Akai,[3] Whitehead and Grant,[4] and Caruthers.[5]

Numerical solutions of the nonlinear steady problem currently are available for subsonic[6] and transonic[7] cascade flows. A numerical model[2] for solving the unsteady equations on a rectilinear-type, body-fitted, and periodic grid (herein called the "cascade" mesh) which spans the extended-blade-passage solution domain was developed as part of the present overall research program. The cascade mesh is not sufficiently detailed to permit an accurate resolution of the unsteady flow in the vicinity of blunt leading or trailing edges, and, hence, previous unsteady response predictions[1,2] have been restricted to subsonic cascades of sharp-edged blades with mean camber lines aligned with the steady flow.

It has been clear from previous work that improvements in the unsteady solution procedure would be required before a practically useful flutter prediction scheme could be realized. Of most immediate concern is the development of solution procedures to treat general blade profiles and the effects of mean incidence. Thus, in the current phase of the larger research program just outlined, the effort has been directed toward understanding and numerically resolving the unsteady flow in the vicinity of blade edges, in particular, blade leading edges. An analytical model-problem study has been conducted to determine the behavior of first-order perturbation solutions in the vicinity of airfoil edges and to guide the development of a numerical solution procedure. In addition, a numerical approximation based on singular perturbation concepts has been developed to resolve the unsteady boundary value problem for cascades of blunt-nosed blades with mean positions situated at incidence relative to the uniform inlet flow. Finally, this numerical approximation has been applied to determine the unsteady flow past a cascade of NACA 0012 airfoils. Numerical results are presented to demonstrate the solution procedure and to illustrate further the effects of blade geometry (including leading-edge curvature), compressibility, and mean incidence on unsteady response.

Governing Equations

Basic equations that describe the flow past a finite-deflection cascade of airfoils undergoing small-amplitude, harmonic vibrations have been derived in Ref. 1. These equations apply to subsonic or transonic flows; i.e., flows with subsonic inlet and exit velocities, but possibly with embedded supersonic regions adjacent to blade surfaces. In the present effort we seek subsonic solutions to the linear unsteady boundary value problem for realistic cascade configurations. In the following discussion all quantities are dimensionless. Lengths have been scaled with respect to blade chord, time with respect to the ratio of blade chord to upstream freestream speed, and pressure with respect to upstream freestream dynamic pressure.

Presented as Paper 81-1290 at the AIAA 14th Fluid and Plasma Dynamics Conference, Palo Alto, Calif., June 23-25, 1981; submitted July 16, 1981; revision received Nov. 24, 1981.

*Principal Scientist, Gas Dynamics and Thermophysics Laboratory. Member AIAA.

Problem Description

We consider isentropic and irrotational flow, with negligible body forces, of a perfect gas past a two-dimensional oscillating cascade (Fig. 1). The blades are undergoing identical small-amplitude harmonic motions at frequency ω and with constant phase angle σ between the motion of adjacent blades. Thin vortex sheets (the unsteady wakes) emanate from the blade trailing edges and extend downstream. Conditions far upstream and downstream of the blade row, blade shape and orientation, and the amplitude, frequency and interblade phase angle of the motion are assumed to be such that the flow is everywhere subsonic and that it remains attached to the blade surfaces.

The displacement of the mth ($m=0, \pm 1, \pm 2,\ldots$) blade is described by

$$\mathcal{R}_m(X,t) = re^{i(\omega t + m\sigma)} + \mathcal{O}(\epsilon^2), \qquad X \text{ on } S_m \tag{1}$$

where $\mathcal{R}_m$ is a vector measuring the displacement of points on the instantaneous position of the mth blade surface, $\mathcal{S}_m$, relative to their mean positions (on S_m), X is a position vector, t is time, and ϵ is a small parameter related to the amplitude of the blade motion. Only rigid motions are considered; i.e., $r = h + \alpha \times R_p$, where h defines the amplitude and direction of blade translations, α defines the amplitude of blade rotations, and R_p is a vector extending from the mean position of the mth axis of rotation to points on the mean position of the mth blade surface. The components h_x, h_y, and α of the vectors h and α are, in general, complex to account for phase differences between the translations in the x and y directions and the rotation. These rigid two-dimensional motions model chordwise, bending, and torsional vibrations of actual rotor blades.

A perturbation approach[1] serves to replace the nonlinear, time-dependent, boundary value problem for the velocity potential, $\hat{\Phi}(X,t)$ by two time-independent boundary value problems for a zeroth-order or steady potential, $\Phi(X)$, and a first-order or unsteady potential, $\phi(X)e^{i\omega t}$. In addition, unsteady boundary conditions can be applied at the mean positions of the blade and wake surfaces, and surface pressure distributions and aerodynamic response coefficients can be evaluated in terms of information prescribed at blade mean positions. The steady potential, assumed to be known in the present study, is a solution of the full potential equation subject to the conditions of flow tangency at blade mean positions and uniform subsonic flow far upstream and downstream of the blade row.

The Unsteady Boundary Value Problem

The unsteady potential is governed by a linear differential equation of the form

$$A^2 \nabla^2 \phi = \frac{D_S^2 \phi}{Dt^2} + (\gamma - 1)\nabla^2 \Phi \frac{D_S \phi}{Dt} + \nabla\left[\frac{\nabla\Phi \cdot \nabla\Phi}{2}\right] \cdot \nabla\phi \tag{2}$$

where D_S/Dt is the convective derivative relative to the mean flow, i.e.,

$$\frac{D_S}{Dt} = \frac{\partial}{\partial t} + \nabla\Phi \cdot \nabla = i\omega + \nabla\Phi \cdot \nabla \tag{3}$$

A is the local speed of sound in the steady flow, and γ is the specific heat ratio of the fluid. The influence of blade shape and steady turning appears in this equation through the variable coefficients [A^2, $(\gamma-1)\nabla^2\Phi$, etc.] which depend on spatial derivatives of the steady potential.

On blade surfaces the first-order flow tangency condition requires that

$$\nabla\phi \cdot n = [i\omega r + \alpha \times \nabla\Phi - (r \cdot \nabla)\nabla\Phi] \cdot n e^{im\sigma}, \qquad \text{on } S_m \tag{4}$$

where n is a unit outward normal vector. The first term on the right-hand side of Eq. (4) is the surface velocity. The other terms account for the effects of blade rotation relative to the mean flow and motion through a varying mean velocity field. Conditions of continuity of pressure and normal velocity component apply across the blade wakes, i.e.,

$$\Delta_m\left(\frac{D_S\phi}{Dt}\right) = 0 \qquad \text{on } W_m$$

$$\Delta_m(\nabla\phi \cdot n) = 0 \qquad \text{on } W_m \tag{5}$$

where the mean positions of the unsteady wakes W_m are assumed to coincide with the steady flow stagnation streamlines, and Δ_m defines a difference across the mth wake; e.g.,

$$\Delta_m\phi = \phi(X^-) - \phi(X^+), \qquad X \text{ on } W_m \tag{6}$$

In general, unsteady disturbances persist far upstream and downstream of the blade row. Far-field disturbances are caused by acoustic waves propagating away from the blade row and counter vorticity shed at blade trailing edges and convected downstream along the blade wakes. To account for such disturbances, analytic solutions to Eq. (2) have been determined for uniform, subsonic, inlet and exit, mean-flow conditions (i.e., $\nabla\Phi = V_{\mp\infty}$ where V is the steady velocity). These solutions are given explicitly in Ref. 1. To within the first-order approximation they can be matched to near-field numerical solutions at finite distances upstream and downstream from the blade row. Finally, the cascade geometry and the prescribed form of the blade motion, Eq. (1), require that the unsteady flow exhibit blade-to-blade periodicity; i.e.,

$$\phi(X) = \phi(X + mG)e^{-im\sigma}, \qquad m = 0, \pm 1, \pm 2,\ldots \tag{7}$$

where the vector G is directed along the locus of blade leading edges with magnitude equal to the blade spacing (Fig. 1). Thus a numerical resolution of a linear, time-independent, unsteady boundary value problem is required only over a single extended-blade-passage region of finite extent.

Aerodynamic Response Coefficients

Solutions to the unsteady boundary value problem are required to determine blade pressure distributions and aerodynamic forces and moments. The unsteady pressure acting at the instantaneous position at the mth blade surface, $p_S e^{i(\omega t + m\sigma)}$, can be evaluated in terms of information determined at the mean position S of the zeroth or reference blade. It follows from Bernoulli's equation and the isentropic

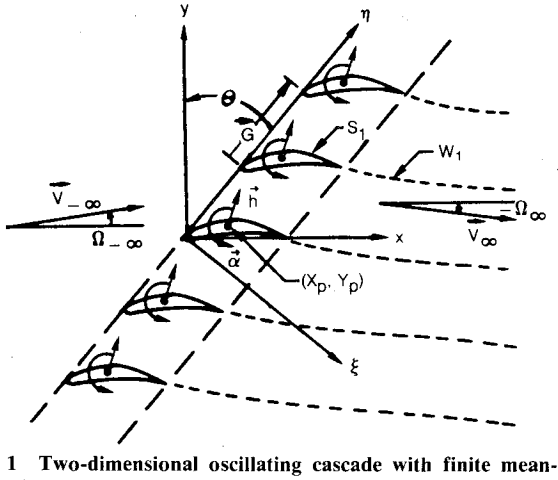

Fig. 1 Two-dimensional oscillating cascade with finite mean-flow deflection.

relations that

$$p_{\mathcal{S}} = \left[-2(M_{-\infty}A)^{2/(\gamma-1)} \frac{D_S \phi}{Dt} + (r\cdot\nabla)P \right]_S \tag{8}$$

where $M_{-\infty}$ is the steady Mach number far upstream of the blade row and P is the steady pressure. The first term on the right-hand side of Eq. (8) determines the unsteady pressure at the blade mean position and the second accounts for motion through a nonuniform steady pressure field. The unsteady force $c_F e^{i(\omega t+m\sigma)}$ and moment $c_M e^{i(\omega t+m\sigma)}$ coefficients are determined by integration over the mean position of the reference blade surface; i.e.,

$$c_F = -\oint_S p_{\mathcal{S}} n ds + \alpha \times C_F, \qquad c_M = \oint_S p_{\mathcal{S}} R_p \cdot \mathbf{d}s \tag{9}$$

where C_F is the steady force coefficient and $\mathbf{d}s$ is a differential vector tangent to the mean blade surface.

Incompressible Model Problem

An understanding of first-order solution behavior is an important prerequisite for a successful numerical resolution of the linear unsteady flow. In addition, certain restrictions are inherent to a perturbation approximation. If these are not satisfied throughout the solution domain, the perturbation expansion is said to be singular; i.e., the asymptotic series does not provide a uniformly valid approximation to the true solution.[8] In classical linear theory this situation is manifested by analytical singularities in the first-order solution at airfoil leading and trailing edges.[9] To clarify both the behavior of the first-order solution and the convergence properties of the asymptotic series associated with the present aerodynamic formulation, especially in the vicinity of a blunt leading edge, a model problem study has been conducted. Exact zeroth- and first-order solutions have been determined and analyzed for an incompressible ($M_{-\infty}=0$), quasisteady ($\omega\to 0$) flow past an isolated ($G\to\infty$) airfoil. Results of this study provide some formal basis for the procedure subsequently adopted for the numerical resolution of unsteady cascade flows.

We consider incompressible flow past an elliptic airfoil $\mathcal{S}$, which has undergone a rigid displacement from an original or mean position S (Fig. 2). The latter is situated at angle of attack Ω relative to the uniform stream V_∞. Body-fixed ξ, η and x,y coordinate axes coincide with the major and minor axes of the ellipses $\mathcal{S}$ and S, respectively. Hence, $z=(z-h)e^{-i\alpha}$ where $z=\xi+i\eta$, and $z=x+iy$; $h=h_x+ih_y$ defines the amplitude and direction of the translational displacement and α defines the amplitude and direction of the rotational displacement about $z=0$. The complex potential $\hat{W}$ for the flow about the displaced ellipse $\mathcal{S}$ is given by[10]

$$(1-b)\,\hat{W}(z) = H(z,\hat{\Omega}) = F(z)\cos\hat{\Omega} + iG(z)\sin\hat{\Omega} + i(1-b)\hat{\Gamma}\ell n\left[\frac{z+\sqrt{z^2-4a^2}}{2}\right] \tag{10}$$

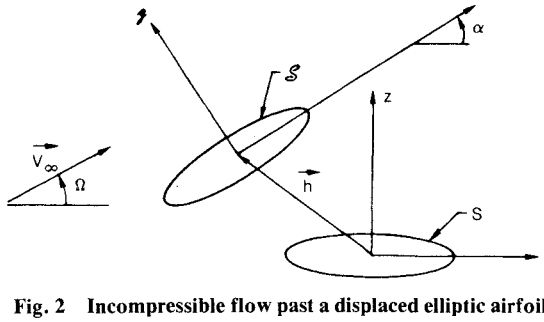

Fig. 2 Incompressible flow past a displaced elliptic airfoil.

where

$$F(z) = z - b\sqrt{z^2-4a^2}, \qquad G(z) = bz - \sqrt{z^2-4a^2}$$

$$\hat{\Gamma} = (1+b)\sin\hat{\Omega}/2 \tag{11}$$

$\hat{\Omega}=\Omega-\alpha$, b is the thickness of the airfoil, $4a=(1-b^2)^{1/2}$ is the distance between the foci (at $\pm 2a$) of the ellipse, and $\hat{\Gamma}$ is the circulation. The circulation has been specified by requiring that the rear stagnation point occurs at the trailing edge ($z=1/2$). For $b=0$, Eqs. (10) and (11) define the complex potential for the flow past a flat plate airfoil. In this case the prescribed circulation guarantees that the flow does not stagnate near the trailing edge of the airfoil (Kutta condition).

The first two terms of an asymptotic series representation for $\hat{W}$; i.e.,

$$\hat{W}(z) = \sum_{j=0}^{\infty} \epsilon^j w_j(z) = W(z) + w(z) + \mathcal{O}(\epsilon^2) \tag{12}$$

are determined explicitly by expanding the second term on the right-hand side of the expression

$$(z^2-4a^2) = (z^2-4a^2)\left[1 + \frac{(z^2-z)^2}{z^2-4a^2}\right] \tag{13}$$

in a binomial series, substituting the result into Eqs. (10) and (11) and neglecting second and higher order terms in h_x, h_y, and α. After some algebra it follows that

$$(1-b)\,W(z) = H(z,\Omega) \tag{14}$$

and

$$(1-b)\,w(z) = -\alpha \frac{\partial H}{\partial \Omega}(z,\Omega) - s\frac{\partial H}{\partial z}(z,\Omega) \tag{15}$$

where $s=h+i\alpha z$. $W(z)$ is the complex potential for the flow past the ellipse S and $w(z)$ is the linear (in h_x, h_y, and α) approximation to the change in this solution due to a rigid displacement. The asymptotic series of Eq. (12) converges to the exact solution of Eq. (10), if $|z^2-z^2| < |z^2-4a^2|$. Thus for sufficiently small displacements ($<\mathcal{O}(b^2/4)$ where $b^2/2$ is the edge radius) the first two terms of this series provide a uniformly valid first-order approximation to the flow past the displaced ellipse.

The velocity potential $\phi = Re\{w(z)\}$ is an exact solution to the first-order boundary value problem discussed in the previous section. Note that for $\omega=0$; $\nabla\phi$ is continuous across the "wake" and disturbances attenuate in the far field; i.e., $\nabla\phi\to 0$ as $|z|\to\infty$. In general, the zeroth- and first-order complex velocities, i.e.,

$$(1-b)\frac{dW}{dz} = \frac{\partial H}{\partial z} \tag{16}$$

and

$$(1-b)\frac{dw}{dz} = -\alpha\frac{\partial^2 H}{\partial\Omega\partial z} - s\frac{\partial^2 H}{\partial z^2} \tag{17}$$

behave like multiples of $z_C^{-1/2}$ and $z_C^{-3/2}$, respectively, near the leading and trailing edges of the airfoil, where z_C is a complex coordinate measured from the focus nearest the edge. Thus for a flat plate airfoil ($b=0$, $a=1/4$), the zeroth- and first order solutions are singular at the edges of the airfoil. However, due to the implementation of the Kutta condition [c.f. Eq. (11)] the order of the singularity is reduced by one (i.e., dW/dz and dw/dz behave like multiples of $z_C^{1/2}$ and $z_C^{-1/2}$, respectively) at a flat plate trailing edge. In addition, for a flat plate at zero mean angle of attack (the classical linear problem) $dW/dz=1$ and the first-order complex velocity behaves like a multiple of $z_C^{-1/2}$ at the leading edge and like a multiple at $z_C^{1/2}$ at the trailing edge.

Inner and Outer Expansions

The foregoing solutions for an elliptic airfoil indicate that zeroth- and first-order flow properties depend on two length scales: the distance from a given point z to the nearest focal point, and the square root of the product of the distances from the point z to the leading and trailing edges; i.e., $(z^2-\frac{1}{4})^{\frac{1}{2}}$. Approximations to the zeroth- and first-order complex velocities, based on this behavior, can be determined as follows. Inner solutions valid in a neighborhood of the leading edge, $|z_C| \sim \mathcal{O}(b^2)$ where $z_C = z+2a$, are obtained by substituting the expansion

$$(z^2-4a^2)^n \sim (-\sqrt{1-b^2})^n z_C^n [1-nz_C/\sqrt{1-b^2}+\mathcal{O}(|z_C|^2)] \tag{18}$$

into Eqs. (16) and (17). It follows after some algebra that for $\Omega \sim \mathcal{O}(b) \ll 1$

$$(1-b)\frac{dW}{dz}\bigg|_I \sim 1+(\Omega-ib/2)z_C^{-\frac{1}{2}}+\mathcal{O}(b^2) \tag{19}$$

and

$$(1-b)\frac{dw}{dz}\bigg|_I \sim s(\Omega-ib/2)z_C^{-3/2}/2-\alpha z_C^{-\frac{1}{2}}+\mathcal{O}(|s|) \tag{20}$$

Thus, as noted earlier, the zeroth- and first-order complex velocities exhibit a $z_C^{-\frac{1}{2}}$ and a $z_C^{-3/2}$ behavior, respectively, in the vicinity of a blunt leading edge. Similar expressions can be determined for the flow in the vicinity of a trailing edge. In this case, the mean angle of attack Ω does not appear as a multiple of the highest order singular terms because of the enforced symmetry, Eq. (11), of the flow at the trailing edge.

Outer solutions valid in the region $|z^2-\frac{1}{4}| \sim \mathcal{O}(1)$ are determined by substituting the expansion

$$(z^2-4a^2)^n \sim (z^2-\tfrac{1}{4})^n [1+nb^2(z^2-\tfrac{1}{4})^{-1}/4]+\mathcal{O}(b^4) \tag{21}$$

into the exact expressions for the zeroth- and first-order complex velocities. It follows for $\Omega \sim \mathcal{O}(b) \ll 1$ that

$$(1-b)\frac{dW}{dz}\bigg|_0 \sim 1-(z^2-\tfrac{1}{4})^{-\frac{1}{2}}[i\Omega(z-\tfrac{1}{2})+bz]+\mathcal{O}(b^2) \tag{22}$$

and

$$(1-b)\frac{dw}{dz}\bigg|_0 \sim \alpha[\Omega-i(1+b)][1-(z-\tfrac{1}{2})^{\frac{1}{2}}(z+\tfrac{1}{2})^{-\frac{1}{2}}]$$

$$+i\alpha b(z^2-\tfrac{1}{4})^{-\frac{1}{2}}/2+s\{(b+i\Omega)(z^2-\tfrac{1}{4})^{-\frac{1}{2}}$$

$$-z[i(z-\tfrac{1}{2})\Omega+bz](z^2-\tfrac{1}{4})^{-3/2}\}+\mathcal{O}(|s|b^2) \tag{23}$$

It can be shown that the outer first-order solution satisfies the first-order boundary value problem [c.f. Eqs. (2), (3), and (4)] when the steady velocity is replaced by the outer approximation to the zeroth-order solution.

Near the leading edge of the airfoil $[z_{LE} \sim \mathcal{O}(b^2)]$ the outer solutions assume the form

$$(1-b)\frac{dW}{dz}\bigg|_0 \sim 1+(\Omega-ib/2)z_{LE}^{-\frac{1}{2}}+\ldots \tag{24}$$

and

$$(1-b)\frac{dw}{dz}\bigg|_0 \sim s(\Omega-ib/2)z_{LE}^{-3/2}/2-\alpha z_{LE}^{-\frac{1}{2}}+\ldots \tag{25}$$

where $z_{LE} = z+\frac{1}{2} = z_C+b^2/4$. Thus the lead terms of the inner and outer expansions have the same functional form near the leading edge of the airfoil. The inner solutions depend on the variable z_C which is measured from the focus at $z=-2a$, while the outer solutions depend on z_{LE} which is measured from the leading edge of the airfoil.

Discussion

The foregoing study reveals several important features of perturbation solutions to airfoil type flows. In particular, the solution for the flow past a displaced airfoil can be represented as an asymptotic series in which the zeroth-order term describes the (nonuniform) flow past the airfoil at its original location and the remaining terms account for the effects of the displacement. This series will converge to the exact solution for the flow past the displaced airfoil if the displacement is small compared to the edge radii of the airfoil. If this criterion is not met, but the displacement is still sufficiently small, the asymptotic series will converge everywhere except near the edges of the airfoil. In this case, the perturbation approximation is singular. In either event, the first-order term of the asymptotic series is a solution of the linear boundary value problem derived by substituting the series into the full governing equations of motion. The zeroth- and first-order solutions are analytic for blunt-edged airfoils, but these potentials, or their derivatives to some order, are singular at sharp leading and trailing edges. Finally, near blade edges, the rapidly varying zeroth- and first-order solutions are essentially functions of a position vector emanating from near the center of the edge circle.

One purpose in conducting the model problem study is to provide guidance for a numerical resolution of unsteady cascade flows. The foregoing analytical results indicate that with the exception of small neighborhoods surrounding the blade edges, the linear unsteady flow could be captured on a rectilinear-type mesh which covers an extended blade passage region. Although this mesh is generally well suited for capturing unsteady phenomena throughout most of the solution domain (i.e., an outer solution), it is not suitable for resolving "inner" phenomena in the vicinity of blunt blade edges. Thus for blunt-nosed blades, the "outer" solution (which is singular at blade edges) should be matched to an inner solution on a dense local mesh surrounding a blade leading edge. A similar procedure could be applied at the trailing edge. However, since viscous phenomena dominate the flow in this region, a detailed inviscid solution near the trailing edge would be of limited practical value.

Calculation of Unsteady Cascade Flows

The numerical solution procedure will be outlined for unsteady subsonic flow through a cascade of airfoils with blunt leading edges and sharp trailing edges. Thus two length scales govern the unsteady solution. Large scale phenomena associated with overall cascade geometry (e.g., stagger angle, gap/chord ratio, blade thickness, etc.) and rigid blade motion will generally scale with blade chord, while small scale phenomena associated with leading-edge curvature will scale with leading-edge radius. Since blade trailing edges are assumed to be sharp and, as a consequence, the mean or steady flow is assumed to satisfy a Kutta condition, local inviscid phenomena associated with trailing-edge curvature and mean flow stagnation near the trailing edge are eliminated from present consideration.

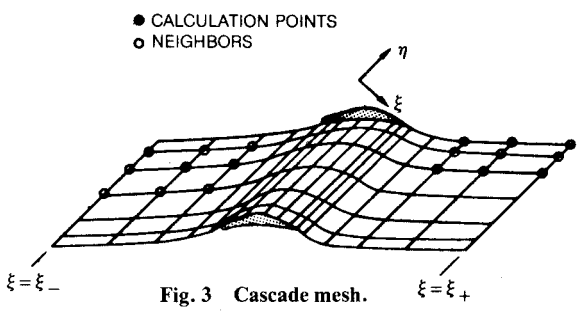

Fig. 3 Cascade mesh.

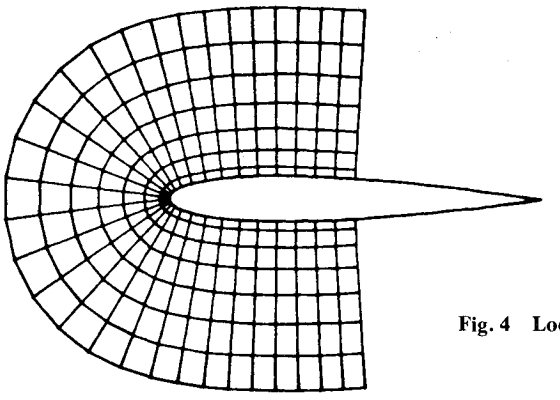

Fig. 4 Local mesh.

Two-Step Solution Procedure

Since it would be difficult to accurately and efficiently approximate both large and small scale unsteady phenomena on a single calculation mesh, a two-step solution procedure has been adopted. Large scale unsteady phenomena are captured on a rectilinear-type (cascade) mesh of moderate density which covers an extended blade passage region, and a small scale phenomena are determined on a polar-type (local) mesh of high density which surrounds the leading edge. The cascade and local mesh solutions then approximate outer and inner solutions, respectively, to the unsteady boundary value problem. The cascade mesh used here is the periodic and body fitted but nonorthogonal one shown schematically in Fig. 3. It is composed of "axial" lines, which are parallel to the blade row making the mesh periodic, and "tangential" curves, which are percentile averages of the upper and lower boundaries making the mesh body fitted. The local mesh is shown in Fig. 4. It is composed of "radial" lines normal to the airfoil surface and "circumferential" lines which roughly parallel the airfoil surface.

In determining an unsteady solution on the cascade mesh inner phenomena due to leading-edge curvature must be excluded from the calculation. Failure to do so can lead to spurious unsteady predictions throughout the solution domain including violent spatial oscillations near blade leading edges. Thus axial and tangential mesh lines should not be placed too close to blade leading edges and the true steady solution near a blunt leading edge should be replaced by an outer approximation to the steady solution. Accurate leading-edge results are then determined by the solution calculated on the local mesh with true steady derivative behavior. Large scale effects are introduced to the local calculation by interpolating the potential calculated on the cascade mesh to the outer radial and circumferential boundaries of the local mesh and imposing the interpolated unsteady potential distribution as an outer boundary condition for the inner solution. The solution to the unsteady boundary value problem is then taken to be the local solution in the region covered by the local mesh and the cascade solution elsewhere.

At present, unsteady solutions have been calculated by the two-step procedure just described in which the local solution is essentially a correction to the cascade solution near the leading edge. Because inner leading-edge effects are not in the cascade calculation, it is necessary to choose the local region extensive enough so that leading-edge curvature effects become insignificant on the local mesh boundaries. This insures that the local boundary value problem has valid information on the outer boundary. It is planned eventually to iterate between cascade and local solutions until the two solutions balance at the interface. When this is done a much smaller local region will suffice.

Numerical Approximations

Solutions on the cascade and local meshes are obtained using finite-difference approximations determined by an implicit interpolation and applicable on arbitrary grids. The implicit interpolation is a linear combination of polynomials with coefficients determined by a weighted least-squares procedure. This difference approximation, which is described in detail in Ref. 2, is flexible enough so that neighbor sets can be adjusted to avoid differencing across singularities—an important feature for the cascade mesh calculation, and so that both differential equation and boundary condition can be simultaneously approximated at boundary points. The latter strategy can significantly improve numerical accuracy in regions where mesh aspect ratios are abnormally large or small.

For the cascade calculation, the neighbor sets are generally defined as shown in Fig. 3; i.e., "centered" neighbor sets are defined at field points, and "one-sided" neighbor sets are defined for points on a blade or wake boundary. In either case, all neighbors fall on the axial mesh line through the calculation point and on the two immediately adjacent axial lines. This placement is important to obtain a desirable structure for the solution matrix. Since derivatives of the unsteady potential exhibit singular behavior at blade edges, either the first point(s) on the blade or the first point off the blade on the upper and lower boundaries of the passage (Fig. 3) is deleted from neighbor sets near blade edges (neighbor set adjustment) to ensure that differences are not taken across singularities. At field points the unsteady differential equation, Eq. (2), is approximated using centered neighbor sets. For points on the upstream upper periodic boundary, ϕ values at neighbors above the mesh region are related to ϕ values at points within the mesh region by the periodic condition, Eq. (7). On the lower periodic boundary the periodic condition is directly applied, since to approximate the field equation on both upper and lower periodic boundaries would be redundant. For points on the far upstream or far downstream boundaries ($\xi=\xi_{\mp}$ in Fig. 3) ϕ values at neighbors upstream and downstream of the mesh region are related to ϕ values on the boundaries using the far-field analytic solutions of Ref. 1. At blade and wake points the flow tangency condition, Eq. (4), and the wake continuity conditions, Eq. (5), are approximated, respectively, using one-sided neighbor sets. At both blade and wake points, the difference equations are constrained to satisfy the field equation.

For the local calculation, matters are much simpler since no special considerations (e.g., neighbor set adjustment) need to be taken at the leading edge and the many types of boundary conditions become only two. Neighbor sets are chosen as for the global calculation, i.e., centered at field points and one-sided at boundary points. The unsteady differential equation and flow tangency condition are approximated as described at field points and blade points, respectively. At points on the outer boundary of the local mesh the unsteady potential is given the value interpolated from the cascade calculation.

Let ϕ_ℓ be a vector of the ϕ values on the ℓth axial mesh line for the cascade calculation or on the ℓth radial mesh line for the local calculation. Because neighbor sets of points on the ℓth line include points only from the lines $\ell-1$, ℓ, $\ell+1$ (and because the cascade calculation mesh is periodic), the systems of linear algebraic equations for both cascade and local calculations s ave the following block tridiagonal form:

$$B_1\phi_1+C_1\phi_2=d_1$$

$$A_\ell\phi_{\ell-1}+B_\ell\phi_\ell+C_\ell\phi_{\ell+1}=d_\ell \qquad 2\le\ell\le L-1$$

$$A_L\phi_{L-1}+B_L\phi_L=d_L \tag{26}$$

With this structure, the systems can be solved directly and efficiently using Gaussian elimination.

Numerical Results

The foregoing procedure has been applied to determine the unsteady flow past a vibrating cascade of NACA 0012 air-

foils. The mean position of the zeroth or reference blade surface is defined by the equation[11]

$$y(x) = \pm 5T[0.2969\sqrt{x} - 0.1260x - 0.3516x^2 + 0.2843x^3 - 0.1015x^4], \qquad 0 \le x \le 1 \tag{27}$$

Here $T = 0.12$ is the thickness and $1.1019T^2$ is the leading-edge radius of the airfoil. For the present application the coefficient of the x^4 term in Eq. (27) has been changed to 0.1036 so that upper and lower surfaces close at $x = 1$ in a wedge-shaped trailing edge. Results have been determined for unstaggered ($\Theta = 0$ deg) and staggered (with $\Theta = 45$ deg) cascades with unit gap/chord ratio ($G = 1$) for prescribed steady inlet Mach numbers ($M_{-\infty}$) and inlet flow angles ($\Omega_{-\infty}$). Corresponding exit Mach numbers (M_{∞}) and flow angles (Ω_{∞}) are determined by a global mass balance and the application of a steady Kutta condition at blade trailing edges.

Unsteady solutions were determined on cascade and local meshes for a blade passage solution domain extending two axial chords upstream and downstream of the blade row. The cascade mesh consisted of 15 tangential and 69 axial lines, 25 of which intersected blade surfaces. The local mesh consisted of 12 circumferential lines which wrapped around the leading edge of the airfoil and extended from normal lines to the upper and lower surfaces at midchord, and 100 normal or radial lines which extended outward from the airfoil to one-half the minimum distance (i.e., the throat) between adjacent blades. A variable mesh spacing has been used in both the cascade and local calculations. Steady flows have been calculated on similar but coarser meshes using the finite area approximation developed by Caspar et al.[6]

Unsteady pressure (p) and pressure difference (Δp) distributions, where

$$\Delta p(x) = p_{s^-}(X) - p_{s^+}(X) = p_{s_I^-}(X+G)e^{-i\sigma} - p_{s_\theta^+}(X) \tag{28}$$

and aerodynamic lift ($c_L = c_F \cdot e_y$) and moment (c_M) coefficients will be presented for blades undergoing single-degree-of-freedom bending [with $h_y = (1,0)$] or torsional (with $\alpha = 1,0$) vibrations. The torsional axis is assumed to be at midchord, $(X_p, Y_p) = (0.5, 0)$. When the imaginary parts of the bending or torsional amplitudes are set equal to zero, the real and imaginary parts of the response coefficients are in phase with blade displacement and velocity, respectively. The stability of single-degree-of-freedom bending motions with $\mathrm{Im}\{h_y\} = 0$ is governed by the sign of the imaginary part of the lift coefficient. If $\mathrm{Im}\{c_L\} < 0$ the airstream tends to suppress the motion and, hence, this motion is stable according to linear theory. Similarly, if $\mathrm{Im}\{\alpha\} = 0$, single-degree-of-freedom torsional motions are stable when $\mathrm{Im}\{c_M\} < 0$ (Ref. 12). In addition to the NACA 0012 cases, for purposes of comparison, numerical results (determined on the cascade mesh) will be presented for oscillating flat plate cascades with blade mean positions aligned parallel to the freestream direction. In this case $\Phi = x$ and the unsteady equations reduce to those of classical small disturbance theory.[9]

Behavior Near Leading Edge

Unsteady surface pressure predictions near the leading edge of the reference NACA 0012 blade are shown in Figs. 5-7 for an unstaggered cascade operating at an inlet Mach number of 0.5. Cascade and local mesh solutions for the unsteady pressure difference distribution due to a unit frequency ($\omega = 1$), out-of-phase ($\sigma = \pm 180$ deg) bending vibration are shown in Fig. 5. Here, the pressure difference is plotted vs the square root of the distance along the airfoil chord from the leading edge. The inlet flow angle is 0 deg and, hence, the steady flow stagnates at the leading-edge point, $x = 0$. A peak steady Mach number equal to 0.667 occurs on the upper and lower airfoil surfaces at $x = 0.152$. The unsteady solution on the cascade mesh approximates an outer solution singularity in Δp at the leading edge, which is removed by the subsequent local solution. The latter determines a zero pressure difference at a blunt leading edge and a local minimum in the real (at $x = 0.004$) and imaginary (at $x = 0.014$) components of the unsteady pressure difference near the leading edge. As indicated in Fig. 5, significant differences exist between the real components of the lift and momentum coefficients predicted by the cascade and the combined (i.e., cascade + local) solutions. However, the outer solution provides a good approximation to the response components (imaginary) in phase with the velocity of the blade motion.

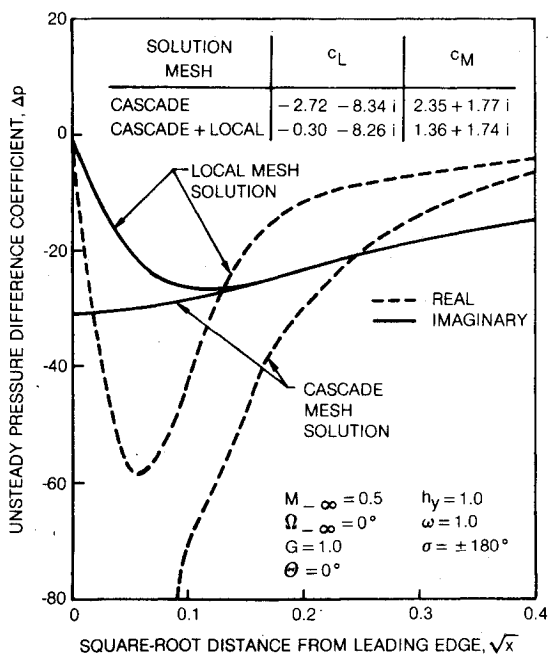

Fig. 5 Unsteady pressure difference near the leading edge of a NACA 0012 blade due to bending.

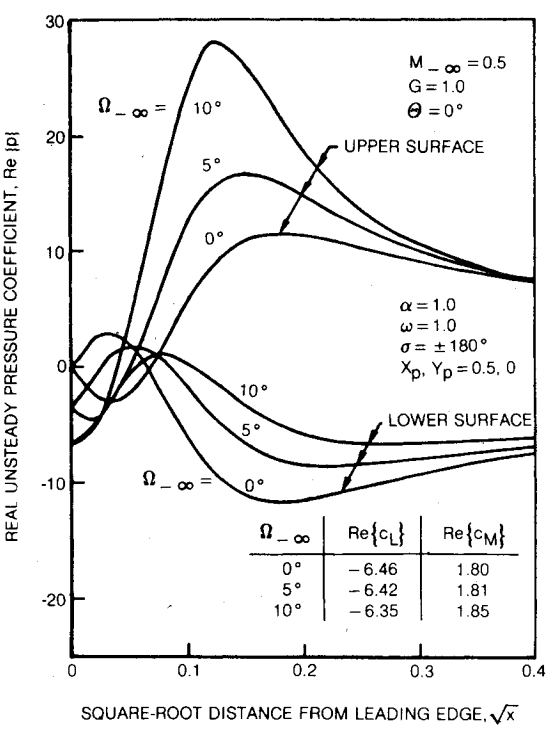

Fig. 6 Effect of incidence on real pressure distribution due to torsion near the leading edge of a NACA 0012 blade.

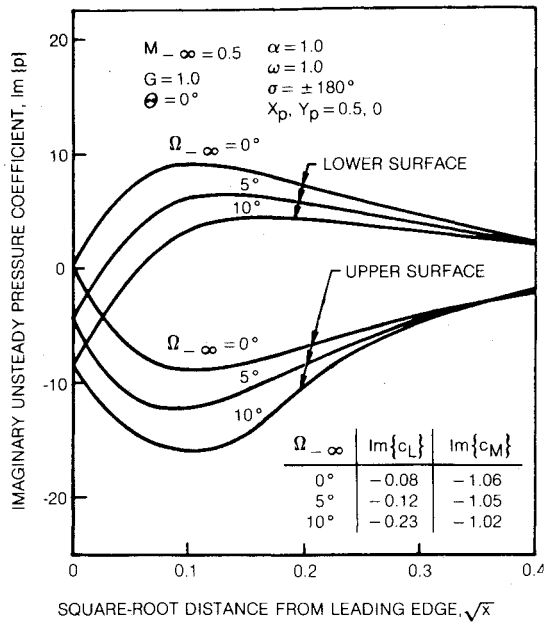

Fig. 7 Effect of incidence on imaginary pressure distribution due to torsion near the leading edge of a NACA 0012 blade.

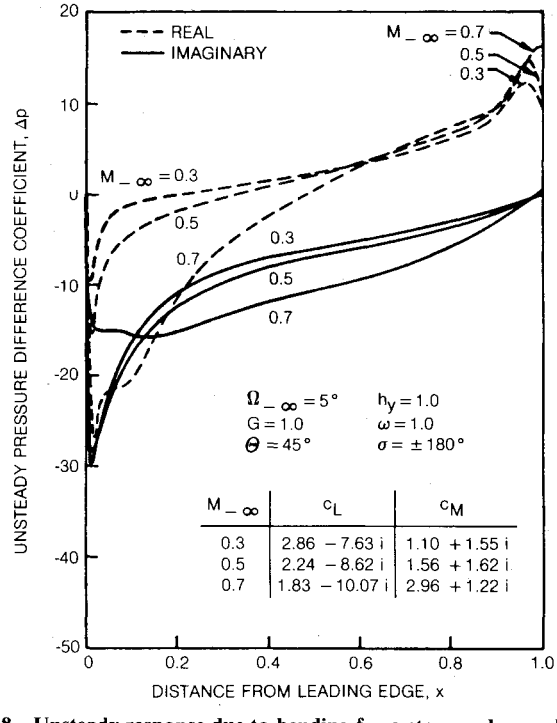

Fig. 8 Unsteady response due to bending for a staggered cascade of NACA 0012 airfoils.

The effect of mean incidence on the response of single-degree-of-freedom motions has been examined by computing unsteady solutions for inlet flow angles of 0, 5, and 10 deg. For $\Omega_{-\infty} = 5$ deg the peak steady Mach number on the suction (upper) surface is 0.734 (at $x = 0.048$) and for $\Omega_{-\infty} = 10$ deg the peak Mach number is 0.885 (at $x = 0.03$). The mean flow stagnates at $x = 0.006$ and $x = 0.01$ on the pressure (lower) surface for $\Omega_{-\infty} = 5$ deg and for $\Omega_{-\infty} = 10$ deg, respectively. The numerical results indicate that an inlet flow angle variation from 0 to 10 deg has little impact on overall unsteady pressure difference distribution, and hence, on unsteady lift and moment coefficient. However, a change in mean incidence angle does cause significant variations in unsteady surface pressure near the leading edge of the airfoil.

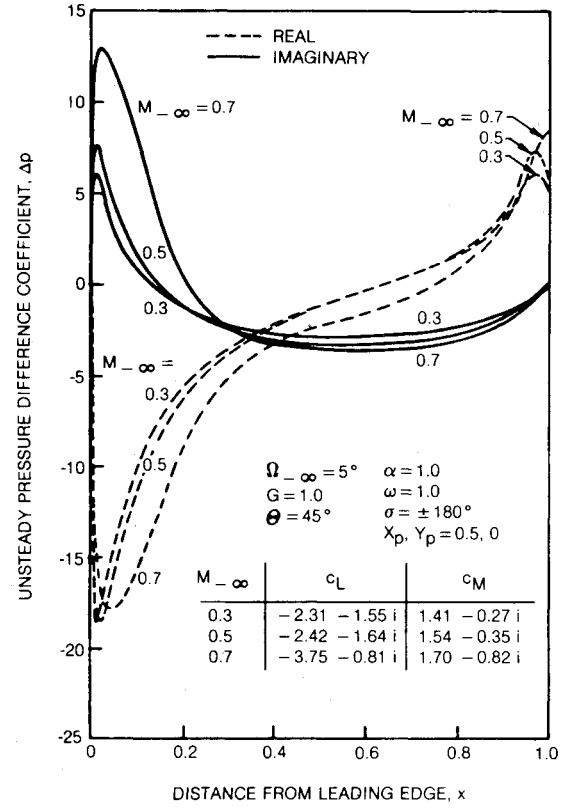

Fig. 9 Unsteady response due to torsion for a staggered cascade of NACA 0012 airfoils.

Real and imaginary unsteady surface pressure distributions near the leading edge of the reference blade are shown in Figs. 6 and 7, respectively, for the torsional case. Although there are substantial differences in unsteady pressure in the immediate vicinity of the leading edge ($0 \le \sqrt{x} \le 0.3$) these do not persist over the entire airfoil, and therefore unsteady force and moment coefficients (e.g., Figs. 6 and 7) are relatively unaffected by changes in inlet flow angle.

Staggered Cascades

Predictions for staggered cascades of NACA 0012 airfoils are shown in Figs. 8 and 9 for a stagger angle of 45 deg and inlet Mach numbers of 0.3, 0.5, and 0.7. The inlet flow angle is 5 deg in each case. Peak steady Mach numbers on the suction surface are 0.379, 0.649, and 0.970 and occur at $x = 0.053$, 0.068, and 0.095, respectively. The steady flows stagnate on the lower surface of the airfoil within a distance of 0.03% of blade chord from the leading edge and the stagnation point moves closer to the leading edge as inlet Mach number increases. Unsteady response predictions for unit frequency, out-of-phase, bending (Fig. 8) and torsional (Fig. 9) vibrations indicate the following trends with increasing inlet Mach number. For bending, the real component of the pressure difference distribution decreases substantially over the forward half of the airfoil leading to a reduction in real lift component and an increase in the real counterclockwise moment. The imaginary component of the pressure difference distribution increases near the leading edge, but decreases over most of the airfoil providing a substantial increase in the magnitude of the force opposing the motion and a reduction in counterclockwise moment at high Mach number. For the torsional case, real pressure differences decrease over most of the blade providing a reduction in lift and an increase in counterclockwise moment. Further, imaginary pressure differences increase on the forward 30% of the blade and decrease over the remainder of the blade, leading to a reduction in lift and an increase in the

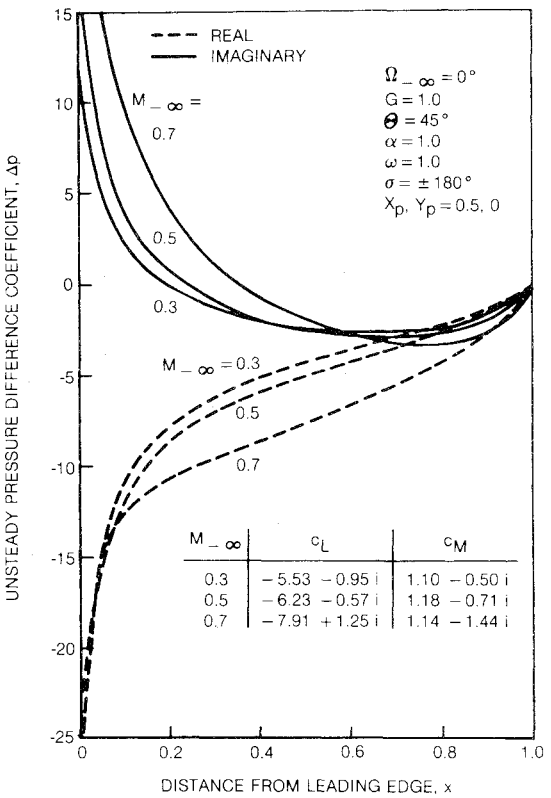

Fig. 10 Unsteady response due to torsion for a staggered flat plate cascade.

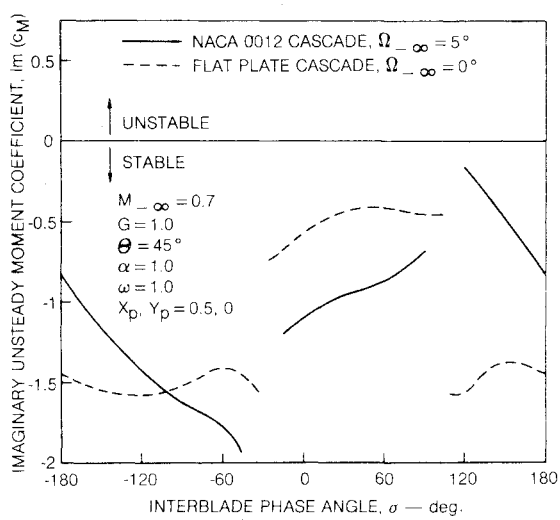

Fig. 11 Imaginary component of unsteady moment due to torsion for staggered cascades.

moment opposing the motion. Hence, the effect of increasing inlet Mach number is to enhance the stability of both motions.

Similar results have been determined for staggered flat plate cascades with $\Omega_{-\infty} = 0$. Response predictions for the bending motion (not shown) indicate a reduction in the imaginary component of the unsteady pressure difference over most of the airfoil and, hence, an increase in the unsteady force opposing the motion with increasing Mach number. Further, there is a substantial increase in $\mathrm{Im}\{\Delta p\}$ due to torsion (Fig. 10) over the front-half of the airfoil, and therefore an increase in the moment opposing the motion as Mach number increases. A comparison between NACA 0012 and flat plate results indicates that blade thickness enhances the aerodynamic stability of the bending motions, but causes a reduction in stability margin for the torsional (c.f. Figs. 9 and 10) motions.

In an effort to briefly examine the effect of blade geometry on overall torsional stability, limited calculations have been performed for the staggered ($\Theta = 45$ deg, $G = 1$) cascades of NACA 0012 and flat plate airfoils undergoing single-degree-of-freedom torsional vibrations about midchord. For these cases the inlet Mach number was set at 0.7. The inlet flow angle was set at 5 deg for the NACA 0012 cascade and at 0 deg for the flat plate configuration. Results were determined for two frequencies, $\omega = 0.5$ and 1.0, over the entire interblade phase angle range (i.e., -180 deg $< \sigma < 180$ deg). Predictions for the imaginary component of the moment coefficient for the unit frequency motions are shown in Fig. 11. Here super-resonant conditions (i.e., acoustic waves persist far upstream and/or far downstream of the cascade)[1] exist for -28.6 deg $< \sigma < 112.4$ deg for the NACA 0012 cascade and for -29.4 deg $< \sigma < 107.3$ deg for the flat plate cascade. The aerodynamic damping (which is proportional to $-\mathrm{Im}\{c_M\}$) for super-resonant motions is greater for the NACA 0012 than for the flat plate blades. However, this situation is dramatically reversed over most of the subresonant region. The maximum calculated values of $\mathrm{Im}\{c_M\}$ for $\omega = 1$ were -0.157 at $\sigma = 120$ deg (subresonant) for the NACA 0012 cascade and -0.408 at $\sigma = 60$ deg (super-resonant) for the "classical" flat plate configuration. Hence, at least for this example, the effect of blade geometry is to cause a substantial reduction in torsional stability margin. In addition, the predictions at the lower frequency ($\omega = 0.5$) indicate that the NACA 0012 cascade will experience a subresonant torsional instability (for 60 deg $< \sigma <$ 125 deg) while the flat plate motions are stable.

Concluding Remarks

The aerodynamic analysis described here has been developed to predict the flow past a finite-deflection, oscillating cascade operating in subsonic freestream conditions. In our previous studies[1,2] unsteady solutions were determined for cascades of sharp-edged blades (i.e., flat plate, thin-circular-arc, and double-circular-arc profiles) with mean camber lines aligned with the steady flow. In this paper, the solution procedure has been extended and applied to cascades of blunt leading-edged airfoils at incidence relative to the inlet flow, and unsteady response predictions have been presented for vibrating cascades of NACA 0012 airfoils.

Detailed local solutions for the NACA 0012 profiles provide unsteady pressure difference distributions which are zero at the leading edge and reach maximum or minimum values at distances from the leading edge on the order of the leading-edge radius. Further, results for unstaggered cascades indicate that mean incidence has only a slight effect on the unsteady force and moment produced by vibrating NACA 0012 airfoils. Finally, predictions for staggered ($\Theta = 45$ deg) NACA 0012 and flat plate cascades reveal a strong influence of inlet Mach number and blade thickness on aerodynamic stability. In particular, the stability of out-of-phase bending or torsional vibrations is enhanced with increasing Mach number for both the NACA 0012 and flat plate cascades, but especially for the former. In addition, the stability margin for unit-frequency, torsional motions at $M_{-\infty} = 0.7$ is substantially less for the NACA 0012 than for the flat plate profiles.

It is not possible to offer general and definitive statements on the stability of practical cascade configurations without performing detailed and extensive parametric studies. However, based on the limited results presented here and in Refs. 1 and 2, some general conclusions can be made on the effects of nonuniform (due to blade geometry and flow turning) mean flow on unsteady aerodynamic response. In particular, blade thickness produces a relatively strong coupling between the steady and unsteady flows, particularly

at high Mach number and low vibration frequency. Further, unsteady surface pressures in the immediate vicinity of a blade leading edge are strongly dependent on inlet flow angle, but in subsonic attached flow this dependence rapidly diminishes with distance from the leading edge. As a result, steady flow turning due to mean incidence or blade camber has only a weak impact on unsteady force and moment. Finally, leading-edge curvature effects must be taken into account to predict accurately unsteady response parameters in phase with blade displacement.

Further developments in the unsteady aerodynamic analysis will be required before a comprehensive flutter prediction scheme can be realized. For the subsonic inlet Mach number range in which blade vibrations are of practical concern, it will be necessary to extend the present analysis to include transonic flows with weak shocks. In addition, for vibrating thin fan or compressor blades at incidence—the positive incidence flutter problem[13]—it appears that the aerodynamic model will have to be modified to incorporate the effects of viscous induced, leading-edge separation bubbles. Moreover, the aerodynamic analysis developed to predict cascade flutter or free vibration phenomena should be combined with solutions of the vorticity and entropy transport equations (c.f. Ref. 14) to provide an analysis for the prediction of forced excitation phenomena in turbomachinery blade rows.

Acknowledgments

This research was sponsored by NASA Lewis Research Center under Contract NAS3-21981. The advice and assistance provided by Dr. John J. Adamczyk, NASA Program Manager for this contract, are gratefully acknowledged.

References

[1] Verdon, J. M. and Caspar, J. R., "Subsonic Flow Past Oscillating Cascade with Finite Mean Flow Deflection," *AIAA Journal,* Vol. 18, May 1980, pp. 540-548.

[2] Caspar, J. R. and Verdon, J. M., "Numerical Treatment of Unsteady Subsonic Flow Past an Oscillating Cascade," *AIAA Journal,* Vol. 19, Dec. 1981, pp. 1531-1539.

[3] Atassi, H. and Akai, T. J., "Effect of Blade Loading and Thickness on the Aerodynamics of Oscillating Cascades," AIAA Paper 78-227, Jan. 1978.

[4] Whitehead, D. S. and Grant, R. J., "Force and Moment Coefficients for High Deflection Cascades," *Aeroelasticity in Turbomachines,* edited by P. Suter, Proceedings of the Second International Symposium held in Lausanne, Switzerland, Sept. 1980, Juris-Verlag Zurich, 1981, pp. 85-127.

[5] Caruthers, J. E., "Aerodynamic Analysis of Cascaded Airfoils in Unsteady Rotational Flow," *Aeroelasticity in Turbomachines,* edited by P. Suter, Proceedings of the Second International Symposium held in Lausanne, Switzerland, Sept. 1980, Juris-Verlag Zurich, 1981, pp. 31-64.

[6] Caspar, J. R., Hobbs, D. E., and Davis, R. L., "Calculation of Two-Dimensional Potential Cascade Flow Using Finite Area Methods," *AIAA Journal,* Vol. 18, Jan. 1980, pp. 103-109.

[7] Ives, D. C. and Liutermoza, J. F., "Second Order Accurate Calculation of Transonic Flow over Turbomachinery Cascades," *AIAA Journal,* Vol. 17, Aug. 1979, pp. 870-876.

[8] Van Dyke, M., *Perturbation Methods in Fluid Mechanics,* Academic Press, New York, 1964, pp. 45-73.

[9] Ashley, H. and Landahl, M., *Aerodynamics of Wings and Bodies,* Addison-Wesley Publ. Co., Inc., Reading, Mass., 1965, pp. 93 and 245-249.

[10] Milne-Thomson, L. M., *Theoretical Hydrodynamics,* The Macmillan Co., New York, 1960, pp. 159-167.

[11] Abbott, I. H. and Von Doenhoff, A. E., *Theory of Wing Sections,* Dover Publ., New York, 1959.

[12] Fung, Y. C., *An Introduction to the Theory of Aeroelasticity,* John Wiley and Sons, Inc., New York, 1955, pp. 166-168.

[13] Mikolajczak, A. A., Arnoldi, R. A., Snyder, L. E., and Stargardter, H., "Advances in Fan and Compressor Blade Flutter Analysis and Predictions," *Journal of Aircraft,* Vol. 12, April 1975, pp. 325-332.

[14] Goldstein, M. E., "Unsteady Vortical and Entropic Distortions of Potential Flows Round Arbitrary Obstacles," *Journal of Fluid Mechanics,* Vol. 89, Pt. 3, 1978, pp. 433-468.